

# Analysis of galaxy kinematics based on Cepheids from the Gaia DR2 Catalogue

V. V. Bobylev<sup>1\*</sup>, A. T. Bajkova<sup>1</sup>, A. S. Rastorguev<sup>2,3</sup>, and M. V. Zabolotskikh<sup>2</sup>

<sup>1</sup>Central (Pulkovo) Astronomical Observatory of RAS, 65/1 Pulkovskoye Chaussee, Saint Petersburg, 196140, Russia

<sup>2</sup>Sternberg Astronomical Institute, Lomonosov Moscow State University, 13 Universitetskii prospekt, Moscow, 119992, Russia

<sup>3</sup>Faculty of Physics, Lomonosov Moscow State University, 1 bldg.2, Leninskie Gory, Moscow, 119991, Russia

Accepted 2021 January 07. Received 2021 January 07; in original form 2020 May 11

## ABSTRACT

To construct the rotation curve of the Galaxy, classical Cepheids with proper motions, parallaxes and line-of-sight velocities from the Gaia DR2 Catalog are used in large part. The working sample formed from literature data contains about 800 Cepheids with estimates of their age. We determined that the linear rotation velocity of the Galaxy at a solar distance is  $V_0 = 240 \pm 3 \text{ km s}^{-1}$ . In this case, the distance from the Sun to the axis of rotation of the Galaxy is found to be  $R_0 = 8.27 \pm 0.10 \text{ kpc}$ . A spectral analysis of radial and residual tangential velocities of Cepheids younger than 120 Myr showed close estimates of the parameters of the spiral density wave obtained from data both at present time and in the past. So, the value of the wavelength  $\lambda_{R,\theta}$  is in the range of [2.4–3.0] kpc, the pitch angle  $i_{R,\theta}$  is in the range of  $[-13^\circ, -10^\circ]$  for a four-arm pattern model, the amplitudes of the radial and tangential perturbations are  $f_R \sim 12 \text{ km s}^{-1}$  and  $f_\theta \sim 9 \text{ km s}^{-1}$ , respectively. Velocities of Cepheids older than 120 Myr are currently giving a wavelength  $\lambda_{R,\theta} \sim 5 \text{ kpc}$ . This value differs significantly from one that we obtained from the samples of young Cepheids. An analysis of positions and velocities of old Cepheids, calculated by integrating their orbits backward in time, made it possible to determine significantly more reliable values of the parameters of the spiral density wave: wavelength  $\lambda_{R,\theta} = 2.7 \text{ kpc}$ , amplitudes of radial and tangential perturbations are  $f_R = 7.9 \text{ km s}^{-1}$  and  $f_\theta = 5 \text{ km s}^{-1}$ , respectively.

**Key words:** stars: distances < Stars, stars: variables: Cepheids < Stars, Galaxy: kinematics and dynamics < The Galaxy, Galaxies, galaxies: spiral < Galaxies

## 1 INTRODUCTION

Cepheids are of great interest because they implement an independent scale of astronomical distances. For these variable stars it is possible thanks to the period–luminosity (Leavitt 1908; Leavitt & Pickering 1912) (PLR) and period–Wesenheit (Madore 1982; Caputo et al. 2000) relations (PWR). Currently, these relations are well calibrated using high-precision trigonometric parallaxes of stars (Ripepi et al. 2019). The use of this relations allows us to estimate the distances to Cepheids with random errors smaller than 10% (Berdnikov et al. 2000; Sandage & Tamman 2006; Skowron et al. 2019). Note that Lazovik & Rastorguev (2020) derived PLR by new method, using multiphase temperature measurements, which made it possible to calculate the most accurate individual color excesses of Cepheids used. The method is based on the

Baade-Becker-Wesselink approach, and practically does not use trigonometric parallaxes.

Classical Cepheids are young (under  $\sim 400$  million years old) supergiant stars with periods of radial pulsations from  $\sim 1$  to  $\sim 100$  days. They are attributed to the flat component of the stellar population of the Galaxy, therefore they are used to study the structural and kinematic features of the galactic disk.

In the works of various authors (Joy 1939; Pont et al. 1997; Metzger et al. 1998), the rotation parameters of the Galaxy were determined using only the distances and line-of-sight velocities of Cepheids.

To determine the Galactic rotation parameters, the combination of distances, line-of-sight velocities, and proper motions of Cepheids was used, for example, in Frink et al. (1995). In this case proper motions from the PPM (Röser & Bastian 1988) catalog, which are not very accurate, were taken.

On the basis of classical Cepheids with proper motions from the Hipparcos Catalog (Hipparcos 1997), there were re-

\* E-mail: vbobylev@gaoran.ru

fined the galactic rotation parameters (Feast & Whitelock 1997; Mel'nik et al. 2015), the parameters of the spiral structure (Mel'nik et al. 1999; Bobylev & Bajkova 2012; Dambis et al. 2015) and the parameters of the galactic disk flexure (Bobylev 2013a,b). Based on Cepheids of II type (the old, low mass counterpart to classical Cepheids), there were determined the parameters of the central bulge and the distance to the galactic center (Majaess et al. 2009).

The measurements obtained by the space experiment Gaia citep Prusti16 are unprecedented in accuracy and volume for the study of the Galaxy. Currently the second version of the Catalog, Gaia DR2, has been published (Brown et al. 2018). The average errors of trigonometric parallaxes of bright stars ( $G < 15^m$ ) in this Catalog lie in the range of 0.02–0.04 milliarcseconds (mas), and for faint stars ( $G = 20^m$ ) they are of the order 0.7 mas. Similarly, the proper motion errors vary from 0.05 mas year<sup>-1</sup> for bright ( $G < 15^m$ ) to 1.2 mas year<sup>-1</sup> for faint ( $G = 20^m$ ) stars. Line-of-sight velocities of more than 7 million stars are measured. For stars of spectral classes F-G-K, the average error of the line-of-sight velocities is about 1 km s<sup>-1</sup>.

The problem of establishing the zero point of parallaxes in the Gaia DR2 Catalog is known. Already Lindegren et al. (2018) has indicated the presence of a possible systematic parallax zero-point offset of  $\Delta\pi = -0.029$  mas in Gaia DR2 relative to the inertial reference frame. Currently, there are several reliable independent estimates of this offset. So, from a comparison of eclipsing binary stars, Stassun & Torres (2018) found  $\Delta\pi = -0.082 \pm 0.033$  mas. This value is confirmed by other authors, in particular, in the analysis of Cepheids  $\Delta\pi = -0.046 \pm 0.013$  mas (Riess et al. 2018a),  $\Delta\pi = -0.049 \pm 0.018$  mas (Groenewegen 2018),  $\Delta\pi = -0.071 \pm 0.038$  mas (Skowron et al. 2019) and asteroseismology  $\Delta\pi = -0.053 \pm 0.009$  mas (Zinn et al. 2019). PMZ and MZ relations were derived by hierarchical Bayesian approach for approximately 400 RR Lyrae stars with optical and NIR photometry and Gaia DR2 data (Muraveva et al. 2019) to give  $\Delta\pi \approx -(0.54 - 0.62)$  mas. Note that the work Riess et al. (2018a) used 50 long-period Cepheids with high-precision photometry performed with the Hubble Space Telescope. In the work Groenewegen (2018), a sample of 452 Classical Cepheids was used and 251 Classical Cepheids was used in the work Skowron et al. (2019).

Skowron et al. (2019) built a three-dimensional map of the distribution of 2431 Cepheids in the Galaxy. For this, the classical Cepheids of the main program OGLE (Optical Gravitational Lensing Experiment, Udalski et al. (1997)), were supplemented by Cepheids from GCVS (General Catalog of Variable Stars, Samus' et al. (2017)), ASAS (All Sky Automated Survey, Pojmański (2002)), and by about 200 Cepheids from the Gaia DR2 Catalog and a number of other sources. Using such biggest sample, these authors specified the parameters of the density distribution of galactic Cepheids using the exponential law, and the parameters of the warped galactic disk. We note their Fig. 3 and Fig. 4, from which it is seen how young Cepheids trace a galactic spiral pattern.

In the work Mróz et al. (2019) performed on 773 classical Cepheids with proper motions and line-of-sight velocities from the Gaia DR2 Catalog, the galactic rotation parameters were determined with the highest accuracy. In particular, the galactic rotation velocity at a solar distance

was found to be  $V_0 = 233.6 \pm 2.8$  km s<sup>-1</sup>, and its first derivative  $V'_0 = -1.34 \pm 0.21$  km s<sup>-1</sup> kpc<sup>-1</sup>. As shown by Bobylev & Bajkova (2012), some of the spiral density wave parameters depend on the Cepheids age. Such a parameter is, for example, the phase of the Sun in a spiral wave. Therefore, it is interesting to determine such parameters using Cepheids of different ages from the latest data.

When analyzing maser sources, Rastorguev et al. (2017) obtained the rotation curve parameters in combination with the Strömberg asymmetry parameters, which allowed us to estimate the exponential scale of the galactic disk under the assumption of marginal stability of the intermediate-age disk. It is interesting to compare the results of this approach in application to the kinematic and position data of a large sample of Cepheids.

In the work of Gnacinski (2019) it has been shown that the rotation velocities of classical Cepheids, obtained in three ways: 1) only from line-of-sight velocities, 2) only from proper motion (Gaia DR2) and 3) from full three-dimensional velocity vector, are located between the flat and Keplerian rotation curves. Using a large sample of Cepheids, Ablimit et al. (2020) estimated the rotation velocity of the Galaxy at the Sun position and found the virial mass of the Galaxy and local dark matter density.

Using large number of stars from Gaia DR2, Kawata et al. (2018) have generated the maps of the rotation velocity,  $V_{circ}$ , and vertical velocity,  $V_z$ , distributions as a function of the Galactocentric radius,  $R$ . In the  $R - V_z$  distribution they found the peak of the  $V_z$  distribution shows wave-like features.

Cepheids, as unique “standard candles”, play an important role in the construction of a universal distance scale due to the presence of the period–luminosity relations. These high-luminosity stars can be detected and studied with large ground-based and space telescopes in disk galaxies up to the distances of 20–30 Mpc. Cepheid distances up to several tens of galaxies, where supernova explosions of type Ia were recorded, have long served as the basis for calibrating the luminosities of these supernovae at their maximum brightness. As a consequence, Hubble diagrams for type Ia cosmological supernovae led to the discovery of the accelerated expansion of the Universe (“dark energy”, see Riess et al. (1998); Perlmutter et al. (1997); Riess et al. (2004); Perlmutter et al. (1999); Schmidt et al. (1998) and others).

The combined use of Hubble diagrams for type Ia cosmological supernovae, data on the CMB anisotropy measured by WMAP and Planck space missions, and the results of study of large-scale distribution of galaxies (BAO – Barionic Acoustic Oscillations) made it possible to set the restrictions on the values of the global cosmological parameters: the contribution of the baryonic and non-baryonic matter and that of the dark energy to the total mass-energy density, as well as the curvature parameter and the equation of state (see the most important recent papers by Betoule et al. (2014); Abbott et al. (2019); Scolnic et al. (2018)).

In the last 5–6 years, strong evidence appeared in favor of a significant discrepancy between the values of the Hubble constant  $H_0$ , determined from the CMB anisotropy and from the redshifts of galaxies and brightest optical “standard candles” – Type Ia supernovae, whose luminosities are based on the Cepheid distances of galaxies. Cepheid meth-

ods lead to systematically higher  $H_0$  values by about 6–7  $\text{km s}^{-1} \text{Mpc}^{-1}$  at a significance level of more than  $4\sigma$ . This problem is now well known as “Hubble tension” (see, for example, Riess et al. (2018b); Verde et al. (2019); Riess et al. (2020) and references therein).

Note that the group of CMB-based estimates is often referred to as “global”, referring to the early Universe, while the Cepheid-based group is called as “local”, referring to the recent-epoch Universe. The reasons for the differences and the ways of solving the “tension” problem are being actively discussed (for example, we found about 750 articles with the mention of the term “Hubble tension” in the abstracts of the papers published during last 5 years). In most works, the problem of Hubble tension is analyzed from the theoretical point of view concerned the properties of dark energy and the refinement of the existing models of the Universe.

However, it is possible that the reason for the Hubble tension can be partly explained by the existence of some systematic errors in the Cepheid distance scales used, though the random relative errors of Cepheid distances are within 10%. The main reason for possible systematics is commonly attributed to the differences in the metallicity of galaxies hosting Cepheids. Sandage & Tamman (2006) discussed this issue in details, but this question is still under numerous debates. The second reason – the systematic errors of different kinds that arise during calibration of PLR by trigonometric parallaxes; some are due to nonlinear conversion of parallaxes to distances, and some – to parallax zero-point offset inherent in the Gaia DR2/EDR3 catalogs discovered in a large number of studies (see discussion above). The PLRs derived by the Baade-Wesselink technique can also be distorted by systematic errors. Additional source of possible errors in the Hubble constant determinations based on the redshifts of galaxies and supernovae stars is an underestimation of the influence of the velocity dispersion of galaxies in galaxy clusters (see, for example, Sedgwick et al. (2021)). All these issues affecting the accuracy of the distance scale, including systematic effects, are discussed in the literature, but for a detailed analysis of the kinematics of the Galactic Cepheids presented in this paper, they do not constitute a serious problem.

The aim of this work is to estimate the rotation parameters of the Galaxy, as well as spiral density wave parameters using a large sample of classical Cepheids of different age with proper motions and line-of-sight velocities taken from the Gaia DR2 Catalog.

## 2 DATA

In this work, we use the data on Classical Cepheids from the works of Mróz et al. (2019) and Skowron et al. (2019).

The Catalog of Skowron et al. (2019) contains distance, age, pulsation period, and the mid-infrared (mid-IR) data from Spitzer (Benjamin et al. 2003; Churchwell et al. 2009) and WISE space telescopes (Wright et al. 2010; Mainzer et al. 2011) for 2431 Cepheids. The distances to these stars,  $r$ , were calculated by Skowron et al. (2019) on the base of MIR PLR of Wang et al. (2018) and mid-infrared light curves, where the influence of the interstellar absorption is much smaller than in optics.

There is a debate concerning period-age relations

(Turner 2012). There are known several calibrations proposed to estimate Cepheid’s mean age. For example, the theoretical calibration performed by Bono et al. (2005) and the calibration by Efremov (2003), obtained by analysis of Cepheids in the Large Magellanic Cloud. To estimate the age of Cepheids Skowron et al. (2019) used the calibration from the paper of Anderson et al. (2016).

We note that such a fundamental property of stars as the rotation (Anderson et al. 2016) is of great importance for the study of the classical Cepheid variable stars. The models by Anderson et al. (2016) include rotation, while some other stellar models (Bono et al. 2005) do not, what makes the Cepheids 1.5 to 2 times younger. It should also be noted that the ages derived by Skowron et al. (2019) were extrapolated from Anderson et al. (2016) for the metal-rich Cepheids.

The catalog of Mróz et al. (2019) contains data on 832 Classical Cepheids. The proper motions and line-of-sight velocities of stars included to the catalog, with appropriate errors, are taken from the Gaia DR2 Catalog. We supplemented the Catalog of Mróz et al. (2019) with estimates of the age of Cepheids from the work of Skowron et al. (2019).

Heliocentric distances to Cepheids were taken from 76–81 columns of the Catalog of Mróz et al. (2019). These, in turn, are taken from the work of Skowron et al. (2019), where they were calculated using MIR PLR of Wang et al. (2018) and mid-infrared light curves, which virtually removes the effects of interstellar extinction.

Apparent stellar magnitudes of Cepheids observed in OGLE program, lie in the range from  $I = 11^m$  to  $I = 18^m$  (Skowron et al. 2019). Therefore, in Mróz et al. (2019) and Skowron et al. (2019) catalogs there is a deficiency of bright and well-studied Cepheids from earlier observations.

According to Skowron et al. (2019) the errors in distances to the Cepheids are  $\sim 5\%$ . Problem is that there may be systematics at play toward certain directions, and at given short and long Galactocentric radii where metallicity and  $R$  (ratio of the total-to-selective extinction) differences may be at play, etc.

Random line-of-sight velocity errors  $e_{V_r}$  usually do not exceed  $10 \text{ km s}^{-1}$ , in average they are  $5 \text{ km s}^{-1}$ . Typical proper motion error of about  $0.1 \text{ mas year}^{-1}$  will give tangential velocity error  $e_{V_t} = 5 \text{ km s}^{-1} (0.1 \cdot 4.741 \cdot r)$  only for heliocentric distances greater than  $10 \text{ kpc}$ . Thus, in our sample, random line-of-sight velocity errors introduce the main contribution to random errors of spatial velocities.

The errors of distances and line-of-sight velocities have been taken from the Catalog of Mróz et al. (2019). Fig. 1 represents a histogram of random line-of-sight velocity errors  $e_{V_r}$  of Cepheids (left-hand panel), and errors of tangential velocities  $e_{V_t}$  of these stars versus the heliocentric distance (right-hand panel). It can be seen from the figure that our approximate estimate is in good agreement with the actual distribution of Cepheid’s random velocity errors.

## 3 METHOD

### 3.1 The Galaxy rotation curve parameters

We use a rectangular coordinate system centered on the Sun. The  $x$  axis is directed towards the Galactic center, the direction of the  $y$  axis coincides with the direction of rotation

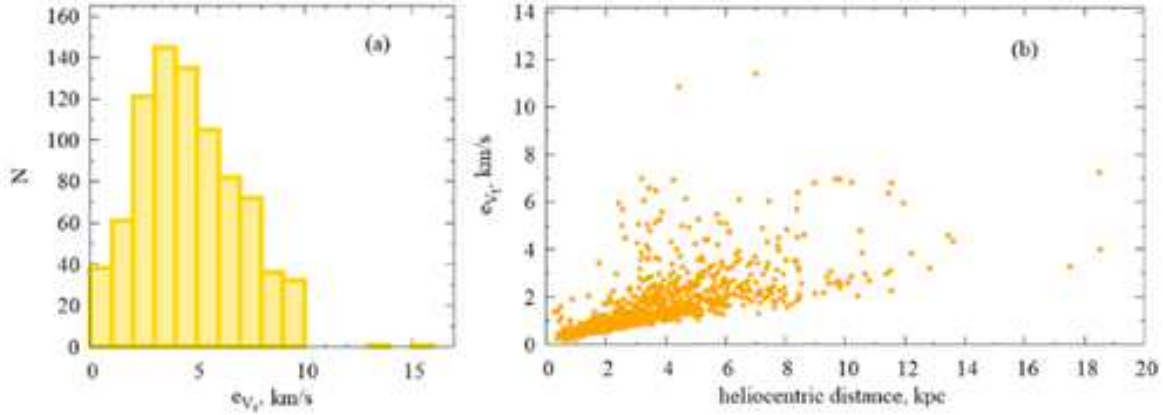


**Figure 1.** A histogram of random errors of line-of-sight velocities of Cepheids (a); errors of the tangential velocities of these stars versus the heliocentric distance (b).

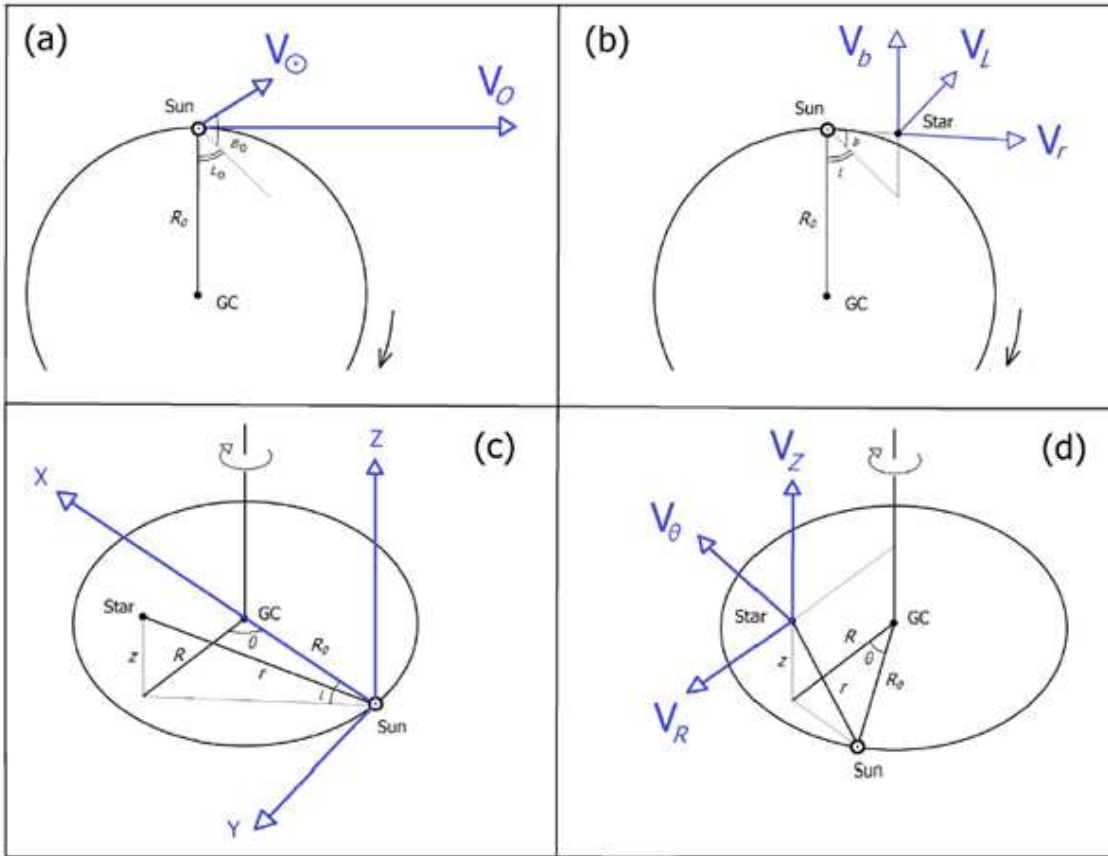


**Figure 2.** The peculiar velocity of the Sun  $V_{\odot}$  and circular rotational velocity of the Sun  $V_0$  around Galactic Center (GC) at distance  $R_0$  (a), the velocity components  $V_r, V_l$  and  $V_b$  (b), coordinate system  $x, y$  and  $z$  (c), cylindrical coordinate system  $V_R, V_{\theta}$  and  $V_z$  (d), thin black arrows indicate the direction of rotation of the Galaxy.

of the Galaxy, and the  $z$  axis is directed towards the north pole of the Galaxy. Then the rectangular coordinates are calculated as follows:  $x = r \cos l \cos b$ ,  $y = r \sin l \cos b$  and  $z = r \sin b$ . This coordinate system is shown in Fig. 2c.

Astrometric observations give three components of a star velocity: the line-of-sight velocity  $V_r$  and two projections of the tangential velocity:  $V_l = 4.74r\mu_l \cos b$  and

$V_b = 4.74r\mu_b$  directed along the galactic longitude  $l$  and latitude  $b$  respectively. All the velocity components are measured in  $\text{km s}^{-1}$ . Proper motion components  $\mu_l \cos b$  and  $\mu_b$  are determined in  $\text{mas year}^{-1}$ . The coefficient 4.741 is equal to the ratio of the number of kilometers in an astronomical unit to the number of seconds in a tropical year, and  $r$  is

the star's heliocentric distance in kpc. The velocities  $V_r, V_l$ , and  $V_b$ , are shown in Fig. 2b.

For stars with known line-of-sight velocities, proper motions and distances, the spatial velocities  $U, V, W$  are calculated as follows:

$$\begin{aligned} U &= V_r \cos l \cos b - V_l \sin l - V_b \cos l \sin b, \\ V &= V_r \sin l \cos b + V_l \cos l - V_b \sin l \sin b, \\ W &= V_r \sin b + V_b \cos b. \end{aligned} \quad (1)$$

Herewith the velocity  $U$  is directed from the Sun to the galactic center,  $V$  is in the direction of galactic rotation and  $W$  is directed to the north galactic pole.

In further studies of the galactic spiral density wave, we also use the following two very important velocities: the radial velocity  $V_R$ , directed from center of the galaxy to the star, and the tangential velocity  $V_{circ}$ , orthogonal to  $V_R$  and directed towards the rotation of the Galaxy, which are calculated using the following formulas:

$$\begin{aligned} V_{circ} &= U \sin \theta + (V_0 + V) \cos \theta, \\ V_R &= -U \cos \theta + (V_0 + V) \sin \theta, \end{aligned} \quad (2)$$

where  $R_0$  is the galactocentric distance of the Sun,  $V_0$  is the linear circular rotation velocity around the galactic center in the solar neighbourhood,  $R$  is the distance from the star to the axis of galactic rotation:

$$R^2 = r^2 \cos^2 b - 2R_0 r \cos b \cos l + R_0^2, \quad (3)$$

and the position angle  $\theta$  meets the relation  $\tan \theta = y/(R_0 - x)$ . Components  $V_R, V_\theta$  (in our case  $V_\theta \equiv V_{circ}$ ) and  $V_z$ , are shown later in Fig. 2d).

We determine the parameters of the galactic rotation curve by solving equations based on Bottlinger's formulas, in which the angular velocity  $\Omega$  is expanded into a Taylor series in powers of  $(R - R_0)$  to the terms of the  $i$ th order of smallness of  $r/R_0$ :

$$\begin{aligned} V_r &= -U_\odot \cos b \cos l - V_\odot \cos b \sin l - W_\odot \sin b \\ &+ R_0 \sin l \cos b \left[ \sum_{i=1}^N (R - R_0)^i \frac{\Omega_0^{(i)}}{i!} \right], \end{aligned} \quad (4)$$

$$\begin{aligned} V_l &= U_\odot \sin l - V_\odot \cos l - r \Omega_0 \cos b \\ &+ (R_0 \cos l - r \cos b) \left[ \sum_{i=1}^N (R - R_0)^i \frac{\Omega_0^{(i)}}{i!} \right], \end{aligned} \quad (5)$$

$$\begin{aligned} V_b &= U_\odot \cos l \sin b + V_\odot \sin l \sin b - W_\odot \cos b \\ &- R_0 \sin l \sin b \left[ \sum_{i=1}^N (R - R_0)^i \frac{\Omega_0^{(i)}}{i!} \right]. \end{aligned} \quad (6)$$

The values  $U_\odot, V_\odot$  and  $W_\odot$  is a group velocities which contain the peculiar motion of the Sun (see Fig. 2a) and the contribution from the effect called "asymmetric drift", which is considered to be small in the case of Cepheids and other young populations. The value  $\Omega_0$  is the angular velocity of the Galaxy at a solar distance  $R_0$ ,  $\Omega_0^{(i)}$  is the  $i$ -th derivative of the angular velocity with respect to  $R$ , the linear rotation velocity at a solar distance equals to  $V_0 = R_0 \Omega_0$ . In the coordinate system  $x, y, z$  shown in Fig. 2c with positive rotation around the  $z$  axis, there will be a rotation from the  $x$  axis to  $y$ . In this case, the sign of the angular velocity  $\Omega$  will be negative, which is not always convenient. We prefer to have a positive  $\Omega$ . Therefore, the equations (4)–(6) are written appropriately (such a coordinate system is shown later).

### 3.2 Residual Velocity Formation

The residual velocities are calculated taking into account the peculiar motion of the Sun,  $U_\odot, V_\odot$  and  $W_\odot$  (see Fig. 2a), as well as the influence of the differential rotation of the Galaxy in the following way:

$$\begin{aligned} V_r &= V_r^* - [-U_\odot \cos b \cos l - V_\odot \cos b \sin l - W_\odot \sin b \\ &+ R_0 (R - R_0) \sin l \cos b \Omega_0' \\ &+ 0.5 R_0 (R - R_0)^2 \sin l \cos b \Omega_0'' + \dots], \end{aligned} \quad (7)$$

$$\begin{aligned} V_l &= V_l^* - [U_\odot \sin l - V_\odot \cos l - r \Omega_0 \cos b \\ &+ (R - R_0) (R_0 \cos l - r \cos b) \Omega_0' \\ &+ 0.5 (R - R_0)^2 (R_0 \cos l - r \cos b) \Omega_0'' + \dots], \end{aligned} \quad (8)$$

$$\begin{aligned} V_b &= V_b^* - [U_\odot \cos l \sin b + V_\odot \sin l \sin b - W_\odot \cos b \\ &- R_0 (R - R_0) \sin l \sin b \Omega_0' \\ &- 0.5 R_0 (R - R_0)^2 \sin l \sin b \Omega_0'' - \dots], \end{aligned} \quad (9)$$

where  $V_r^*, V_l^*, V_b^*$  standing on the right-hand sides of the equations are the initial velocities, and on the left-hand sides there are the corrected velocities  $V_r, V_l, V_b$  which can be used for calculation of the residual velocities  $U, V, W$  by the formulas (1).

The original spatial velocities of stars usually contain a small percentage of values that differ significantly from the average. Such velocities should be discarded using some criterion. Fig. 3 shows the Cepheids  $U, V$  velocities calculated using the relations 1. All Cepheids (820 stars) were used to build this picture without any preliminary rejection. We see that before analyzing such velocities in order to detect rebounds, they must be corrected for the differential rotation of the Galaxy.

Note that the application of the rotation curve obtained on the basis of the equations (4)–(6) has a restriction on  $R$  (Fig. 4). Therefore, for purposes such as detecting bounces when analyzing the residual tangential velocities  $|\Delta V_{circ}|$ , we can simply use the flat rotation curve,  $V_{circ} = const$ . The velocities  $W$  and  $V_R$  do not depend on the rotation curve of the Galaxy (see (2)). As a result, to remove bounces from the sample, we apply the following restrictions:

$$\begin{aligned} |V_R| &< 90 \text{ km s}^{-1}, \\ |\Delta V_{circ}| &< 90 \text{ km s}^{-1}, \\ |W| &< 60 \text{ km s}^{-1}. \end{aligned} \quad (10)$$

Note that the criteria (10) are only used for a preliminary cleaning of the sample, while another rejection criterion (velocity residuals in excess of 3 sigma) will be applied in the analysis.

It is known that the movement of gas and young stars is influenced by the Central galactic bar (Chemin et al. 2019). Some authors refer to the bar as a structure with a half length of 2.5 kpc with a position angle of 15–30 degrees with respect to the Sun-Galactic Centre direction (Babusiaux & Gilmore 2005; Lopez-Corredoira et al. 2005), other researchers suggest that there is a long massive bar with a half length of 4–5 kpc and a position angle of around 45 degrees (Hammersley et al. 1994; Wegg et al. 2015). Moreover, according to some authors (Alard 2001; Nishiyama et al. 2005), there is also a very small inner bar embedded to very central bar/bulge structure with a different orientation as compared to the other two bars.

The strongest influence (deviations from the flat rotation curve more than  $\sim 50 \text{ km s}^{-1}$ , an increase in ve-

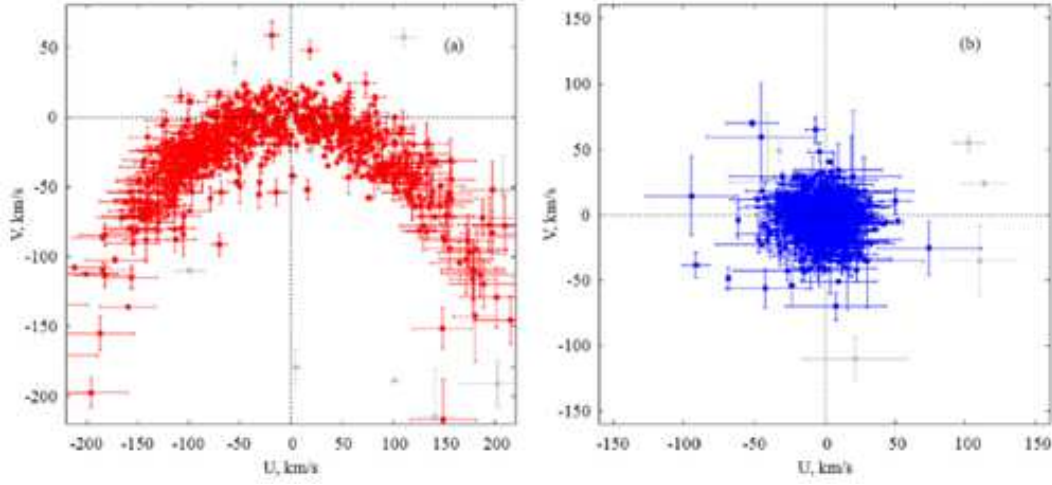


**Figure 3.** Cepheid’s  $U, V$  velocities: not corrected (a) and corrected (b) for the differential galactic rotation; gray symbols indicate stars that were discarded according to the restrictions (10).

locity dispersions) on the velocity of objects due to the bar is observed in the region of 1.5–2 kpc (Clemens 1985; Bhattacharjee et al. 2014; Bajkova & Bobylev 2016), a weak gravitational influence can be traced up to 5 kpc (Chemin et al. 2019). To exclude the influence of the bar, it is advisable to apply the restriction  $R > 2.5$  kpc as an initial condition. As can be seen from Fig. 4 and Fig. 5, practically almost all the Cepheids we use for the kinematical analysis lie at the distances  $R > 4$  kpc.

In the Catalog of Mróz et al. (2019), some Cepheids are located very far from the Galaxy center, at  $r > 25$  kpc, which are also better to exclude from consideration since at large distances proper motion error of about 0.1 mas year<sup>-1</sup> will lead to tangential velocity error  $e_{V_t} > 10$  km s<sup>-1</sup> (see Fig. 1b). As a result of the above restrictions, no more than 20 stars are discarded. The total sample contains 800 Cepheids.

### 3.3 The Spectral Analysis

According to the linear theory (Lin & Shu 1964), the influence of the spiral density wave on the radial  $V_R$  and residual tangential velocities  $\Delta V_{circ}$  has the character of a periodic functions and is described by the following relations:

$$\begin{aligned} V_R &= -f_R \cos \chi, \\ \Delta V_{circ} &= f_\theta \sin \chi, \end{aligned} \quad (11)$$

where  $f_R$  and  $f_\theta$  are positive definite amplitudes of the perturbations of the radial and residual tangential velocities, respectively;

$$\chi = m[\cot(i) \ln(R/R_0) - \theta] + \chi_\odot \quad (12)$$

is the phase of the spiral wave, where  $m$  is the number of spiral arms,  $i$  is a pitch angle of the spiral pattern,  $\chi_\odot$  is a radial phase of the Sun in a spiral wave. As an analysis of modern high-precision data showed, the periodicities associated with a spiral density wave also appear in vertical velocities  $W$  (Bobylev & Bajkova 2015; Rastorguev et al. 2017).

To identify periodicities in the velocities  $V_R$  and  $\Delta V_{circ}$ , we use a modified spectral (periodogram) analysis

(Bajkova & Bobylev 2012). Wavelength  $\lambda$  (distance between adjacent pieces of spiral arms, counted along the radial direction) is calculated as follows:

$$\frac{2\pi R_0}{\lambda} = m \cot(i). \quad (13)$$

Let there be a series of measured velocities  $V_{R_n}$  (these can be  $V_R$  or  $\Delta V_{circ}$  velocities),  $n = 1, \dots, N$ , where  $N$  is a number of objects. The task of spectral analysis is to extract the periodicity from a data series in accordance with the accepted model describing a spiral density wave with parameters  $f, \lambda$  (or  $i$ ) and  $\chi_\odot$ .

As it was shown by Bajkova & Bobylev (2012), taking into account the logarithmic nature of the spiral density wave, as well as the positional angles  $\theta_n$  of objects, our spectral analysis of the series of velocities can be reduced to calculating of the power spectrum of the standard Fourier transform :

$$\bar{V}_{\lambda_k} = \frac{1}{N} \sum_{n=1}^N V'_n(R'_n) \exp\left(-j \frac{2\pi R'_n}{\lambda_k}\right), \quad (14)$$

where  $\bar{V}_{\lambda_k}$  is the  $k$ -th harmonic of the Fourier transform with the wavelength  $\lambda_k = D/k$ ,  $D$  is the period of the analyzed series;

$$\begin{aligned} R'_n &= R_0 \ln(R_n/R_0), \\ V'_n(R'_n) &= V_n(R'_n) \times \exp(jm\theta_n). \end{aligned} \quad (15)$$

The peak value of the power spectrum  $S_{peak}$  corresponds to the desired wavelength  $\lambda$ . The pitch angle of the spiral density wave can be found from (13). We find the amplitude and phase of the perturbations as a result of fitting the harmonics with the found wavelength to the measured data. To estimate the amplitude of disturbances, we use the relation:

$$f_R(f_\theta) = 2 \times \sqrt{S_{peak}}. \quad (16)$$

### 3.4 The choice of the $R_0$ value

Currently, a number of works devoted to determining the average value of the Sun galactocentric distance have been

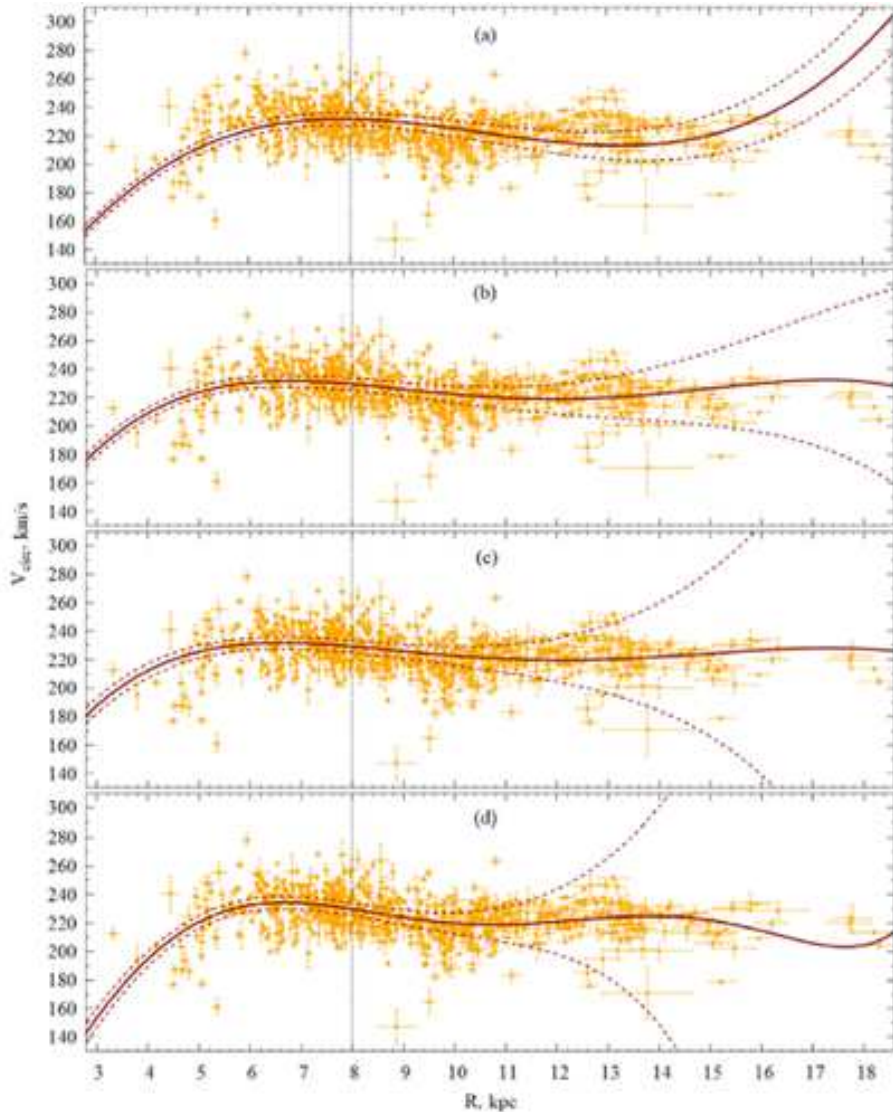


**Figure 4.** The rotation velocities of Cepheids  $V_{circ}$  versus the distance  $R$ , the galaxy rotation curve found from these stars with two derivatives of the angular velocity of rotation (a), with three derivatives (b), with four derivatives (c) and with five derivatives (g); for each curve, the confidence interval limits corresponding to the error level of  $1\sigma$  are marked with dashed lines; all curves are calculated for the accepted value of  $R_0 = 8$  kpc. The vertical line marks the position of the Sun.

performed using individual definitions of this quantity, obtained in the last decade by independent methods.

We note several important results derived as an average over a large number of independent estimates of  $R_0$ . For instance,  $R_0 = 8.0 \pm 0.2$  kpc (Vallée 2017a),  $R_0 = 8.3 \pm 0.4$  kpc (Grijs & Bono 2017) or  $R_0 = 8.0 \pm 0.15$  kpc (Camarillo et al. 2018).

We also note some of the first-class individual definitions of this quantity made recently. In the work of Abuter et al. (2019), from the analysis of a 16-year-long series of observations of the motion of the S2 star around a super-massive black hole in the center of the Galaxy, the value  $R_0 = 8.178 \pm 0.022$  kpc was found. In the work of Do et al. (2019), based on an independent analysis of the orbit of star S2, the value  $R_0 = 7.946 \pm 0.032$  kpc was found. Using data on galactic masers obtained with the Japanese program VERA (VLBI Exploration of Radio Astrometry)

received an estimate of  $R_0 = 7.9 \pm 0.3$  kpc (Hirota et al. 2020). Estimates obtained from the analysis of variable stars are also of interest. From the analysis of VVV-based (VISTA Variables in the Via Lactea) near-infrared RR Lyrae data Majaess et al. (2018) obtained  $R_0 = 8.30 \pm 0.36$  kpc. From the analysis of OGLE-based RR Lyrae data Griv et al. (2020) obtained  $R_0 = 8.28 \pm 0.14$  kpc.

Based on the above results, in the present work we assume the value  $R_0 = 8.0 \pm 0.15$  kpc in cases where  $R_0$  is not a definable parameter.

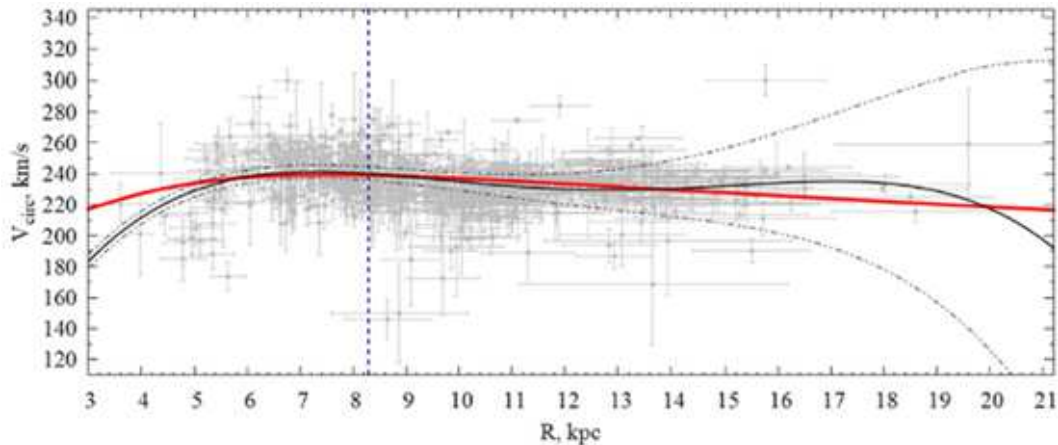


**Figure 5.** The rotation velocities of Cepheids  $V_{circ}$  versus the distance  $R$ ; the thin solid line shows the Galaxy rotation curve found from these stars (solution (17)), the wide red line shows the rotation curve corresponding to the potential model III (Bajkova & Bobylev 2016). The confidence interval limits corresponding to the error level of  $1\sigma$  are marked with dashed lines. The vertical line marks the position of the Sun.

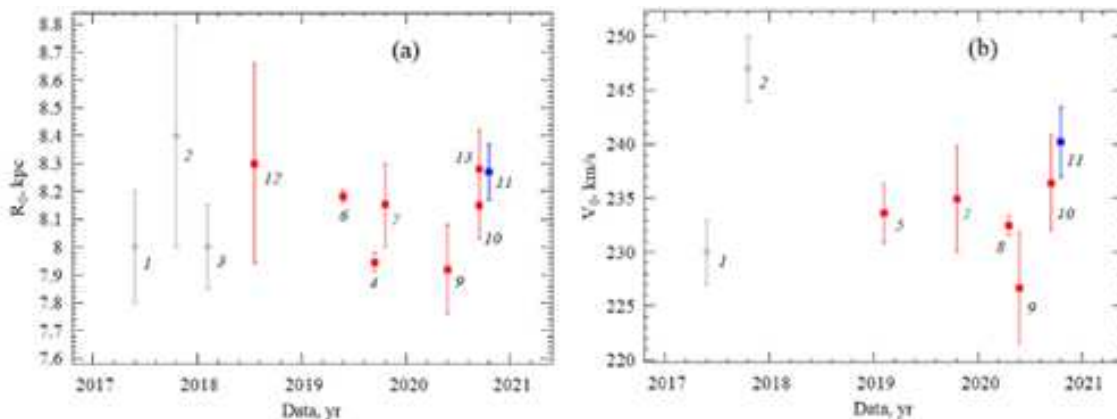


**Figure 6.** The results of determining the distance  $R_0$  (a) and velocity  $V_0$  (b) by various authors depending on the date of publication, gray color indicates the results obtained as an average, red — individual determinations, blue — the result of this work, see also the text.

## 4 RESULTS AND DISCUSSION

### 4.1 Galaxy Rotation

The system of conditional equations (4)–(6) has been solved by the least squares method with weights of the form inversely proportional to random velocity errors, with discarding residuals by the criterion of three sigma.

As can be seen from the Fig. 4, with an increase in the delineable unknowns, the confidence region significantly expands with increasing  $R$ . The rotation curve is close to flat one, which is in good agreement with the conclusion of Mróz et al. (2019). Note that in the Catalog of Mróz et al. (2019) there is a “flag” parameter indicating whether the star was used in kinematic analysis. The criteria of Mróz et al. (2019) are more stringent as compared to (10), since it leaves only 773 stars in the sample. Our sample contains about 800 Cepheids with estimates of their age. After applying all the rejection criteria, our final sample contains 788 Cepheids.

Of the four cases presented in the figure, it is better to choose the option in which the rotation curve is closest to flat one in order to provide the most accurate spectral analysis

of the residual velocities with a minimum of false waves. So in Fig. 4(a) and the curve goes up too early (at  $R \sim 13$  kpc). The curve in Fig. 4(d) seems to better fit the data around 12–13 kpc, but indeed with a wider confidence interval and unnecessary wiggles at large Galactocentric distances. As a result, the rotation curves shown in Fig. 4 (b) and Fig. 4 (c) can be used to obtain the residual Cepheid velocities  $\Delta V_{circ}$  for the purpose of their spectral analysis.

For the entire sample of 788 Cepheids the following kinematic parameters were found:

$$\begin{aligned}
 (U_{\odot}, V_{\odot}, W_{\odot}) &= \\
 (10.1, 13.6, 7.0) \pm (0.5, 0.6, 0.4) \text{ km s}^{-1}, \\
 \Omega_0 &= 29.05 \pm 0.15 \text{ km s}^{-1} \text{ kpc}^{-1}, \\
 \Omega'_0 &= -3.789 \pm 0.045 \text{ km s}^{-1} \text{ kpc}^{-2}, \\
 \Omega''_0 &= 0.722 \pm 0.027 \text{ km s}^{-1} \text{ kpc}^{-3}, \\
 \Omega'''_0 &= -0.087 \pm 0.007 \text{ km s}^{-1} \text{ kpc}^{-4}, \\
 R_0 &= 8.27 \pm 0.10 \text{ kpc}
 \end{aligned} \tag{17}$$

where the error of the unit of weight  $\sigma_0 = 12.4 \text{ km s}^{-1}$ , the Galaxy rotation velocity  $V_0 = 240.2 \pm 3.2 \text{ km s}^{-1}$ . Note that



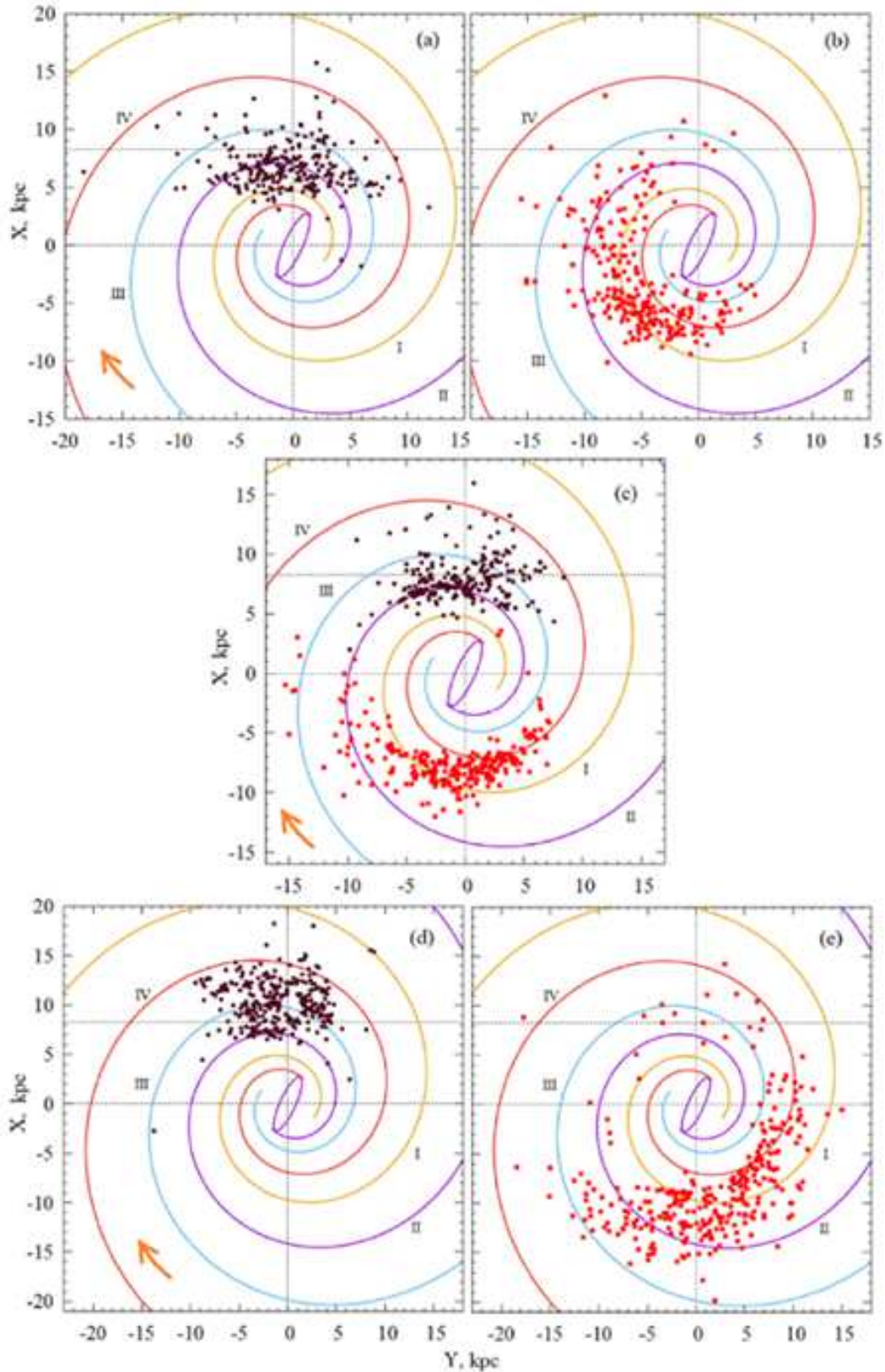


**Figure 7.** The distribution on the galactic plane  $X, Y$  of the youngest Cepheids at the present time (a) and in the past according to the age of each star (b), middle-aged Cepheids (c), samples of old Cepheids at the present time (d) and in the past (e), a four-arm spiral pattern with a pitch angle of  $-13^\circ$  (Bobylev & Bajkova 2014) is given, the spiral arms are numbered in Roman numerals, the orange arrow shows the direction of the Galaxy rotation, the purple dots represent the current positions of the Cepheids, and the red dots represent their positions in the past.

the solution (17) was obtained in such a way that  $R_0$  was also considered the unknown variable. The rotation curve with parameters (17) is shown in Fig. 5.

Based on a sample of 147 masers with trigonometric parallaxes, Reid et al. (2019) found the following values of the two most important kinematic parameters:  $R_0 = 8.15 \pm 0.15$  kpc and  $\Omega_\odot = 30.32 \pm 0.27$  km s<sup>-1</sup> kpc<sup>-1</sup>, where  $\Omega_\odot = \Omega_0 + V_\odot/R$ . The velocity  $V_\odot = 12.24$  km s<sup>-1</sup> was taken from Schönrich et al. (2010)). Reid et al. (2019) used the expansion of the linear Galactic rotation velocity into a series.

Based on a similar approach, Hirota et al. (2020) obtained the following estimates from analysis of 99 masers that were observed within the VERA program:  $R_0 = 7.92 \pm 0.16$  (stat.) $\pm 0.3$  (syst.) kpc and  $\Omega_\odot = 30.17 \pm 0.27$  (stat.) $\pm 0.3$  (syst.) km s<sup>-1</sup> kpc<sup>-1</sup>, where  $\Omega_\odot = \Omega_0 + V_\odot/R$ , and the velocity  $V_\odot = 12.24$  km s<sup>-1</sup> was also taken from Schönrich et al. (2010).

Based on 239 Galactic masers with measured trigonometric parallaxes, Bobylev et al. (2020) found the solar velocity components  $(U_\odot, V_\odot, W_\odot) = (7.79, 15.04, 8.57) \pm (1.25, 1.25, 1.21)$  km s<sup>-1</sup> and the following parameters of the Galactic rotation curve:  $\Omega_0 = 29.01 \pm 0.33$  km s<sup>-1</sup> kpc<sup>-1</sup>,  $\Omega'_0 = -3.901 \pm 0.069$  km s<sup>-1</sup> kpc<sup>-2</sup>,  $\Omega''_0 = 0.831 \pm 0.032$  km s<sup>-1</sup> kpc<sup>-3</sup>, and  $V_0 = 236.4 \pm 4.4$  km s<sup>-1</sup> for the value of  $R_0 = 8.15 \pm 0.12$  kpc found.

Using a sample of 773 Classical Cepheids with precise distances coupled with proper motions and line-of-sight velocities from Gaia DR2, Mróz et al. (2019) constructed the rotation curve of the Milky Way up to the distance of  $R \sim 20$  kpc. These authors found the rotation velocity of the Sun  $V_0 = 233.6 \pm 2.8$  km s<sup>-1</sup> for adopted  $R_0 = 8.122 \pm 0.031$  kpc. It should be noted that the rotation velocity  $V_0$  found by us (17) is in very good agreement with the result of the work Mróz et al. (2019), obtained from the analysis of practically the same stars.

In a recent work by Ablimit et al. (2020), around 3,500 classical Cepheids from various sources, including Mróz et al. (2019) and Skowron et al. (2019), were used to construct the rotation curve of the Galaxy over the distance interval  $R = 4 - 19$  kpc. The circular rotation velocity of the solar neighborhood was obtained equal to  $V_0 = 232.5 \pm 0.9$  km s<sup>-1</sup> (for adopted  $R_0 = 8.122 \pm 0.031$  kpc), which is in good agreement with our estimate.

Further, we assume that the true  $r_t$  and the adopted distance  $r$  are related as  $r_t = r/p$ , where  $p$  is the distance-scale correction factor. The value of the coefficient  $p$  is determined by the internal agreement of the data. Namely, by the agreement of the line-of-sight and tangential velocities. There are two ways to search for the value of the coefficient  $p$ : either by solving the basic kinematic equations (4)–(6) where it will act as an unknown (Rastorguev et al. 2017), or by comparing the values of the first derivative  $\Omega'_0$  obtained only from the analysis of line-of-sight velocities,  $\Omega'_0(r)$ , and only tangential velocities,  $\Omega'_0(\mu)$ , than  $p = \Omega'_0(\mu)/\Omega'_0(r)$  (Zabolotskikh et al. 2002).

We defined the value of the factor  $p$  both for the entire sample and for subsamples of different ages. As a result, we found that the coefficient  $p$  always has approximately the same value, equal to  $\sim 0.9$ . On this basis, it is concluded that the distances  $r$  of the analyzed Cepheids, calculated on

the basis of the period-luminosity relation, must be extended by about 10%.

The results of determining the  $R_0$  and  $V_0$  by various authors are given in Fig. 6, where the results are marked with the following numbers: (1) – Vallée (2017a), (2) – Grijs & Bono (2017), (3) – Camarillo et al. (2018), (4) – Do et al. (2019), (5) – Mróz et al. (2019), (6) – Abuter et al. (2019), (7) – Reid et al. (2019), (8) – Ablimit et al. (2020), (9) – Hirota et al. (2020), (10) – Bobylev et al. (2020), (12) – Majaess et al. (2018), (13) – Griv et al. (2020), (11) – this work.

Fig. 5 gives two rotation curves. One corresponds to solution (17). The second curve corresponds to the axisymmetric gravitational potential model III (a modified NFW model) from the work of Bajkova & Bobylev (2016):

$$V_{circ}^2 = \frac{M_b R^2}{(R^2 + b_b^2)^{3/2}} + \frac{M_d R^2}{[R^2 + (a_d + b_d)^2]^{3/2}} + M_h \left[ \frac{\ln(1 + R/a_h)}{R} - \frac{1}{R + a_h} \right] + const, \quad (18)$$

where,  $M_b$ ,  $M_d$  and  $M_h$  are the masses of the bulge, disk and halo respectively,  $b_b$ ,  $a_d$ ,  $b_d$  and  $a_h$  are the scale lengths (in kpc) of the corresponding galactic components. The gravitational potential is expressed in units of 100 km<sup>2</sup> s<sup>-2</sup>, the lengths in kpc, and the masses in galactic mass units  $M_g = 2.325 \times 10^7 M_\odot$  providing the value of the gravitational constant  $G = 1$ . The term *const* is needed here to accurately match the solar rotation velocity  $V_0$  in this work and in the work of Bajkova & Bobylev (2016) (*const* =  $-4.8$  km<sup>2</sup> s<sup>-2</sup>).

To construct a curve, it is necessary to substitute the following values of seven parameters into this formula (18):  $M_b = 44300$  ( $M_g$ ),  $b_b = 0.2672$  kpc,  $M_d = 279800$  ( $M_g$ ),  $a_d = 4.40$  kpc,  $b_d = 0.3084$  kpc,  $M_h = 1247400$  ( $M_g$ ),  $a_h = 7.7$  kpc.

For spectral analysis of residual circular velocities  $\Delta V_{circ}$  it is important that they are obtained with a relatively smooth rotation curve. As can be seen from Fig. 5, the curve (18) can be used to obtain residual circular velocities in a very wide range of distances  $R > 4$  kpc. The applicability of the rotation curve corresponding to the solution (17) is limited by the interval  $R : 4 - 20$  kpc. In spectral analysis, we use both of the rotation curves described above for mutual control.

## 4.2 Spiral Density Wave Parameters

Spectral analysis was performed for Cepheids of three samples of different ages. The age boundaries were chosen so to ensure approximately equal number of stars in the samples. For each sample, the spiral density wave parameters were obtained for two cases. In the first case, spectral analysis was performed for the present moment in time. In the second case, the position and speeds of each Cepheid were taken at the time of their birth. That is, a galactic orbit in the past was constructed for each star in accordance with an estimate of its age. To construct galactic orbits in the past, an axisymmetric model of the gravitational potential of the Galaxy was used (a modified NFW model from Bajkova & Bobylev (2016)).

The first sample contains 254 stars satisfying the con-

**Table 1.** The parameters of the spiral density wave found from samples of Cepheids from three age intervals for the present moment of time

Parameters	$t < 90$ Myr	$t : 90 - 120$ Myr	$t > 120$ Myr
$\lambda_R$ , kpc	$2.5 \pm 0.3$	$3.0 \pm 0.6$	$5.1 \pm 1.1$
$f_R$ , km s <sup>-1</sup>	$12.0 \pm 2.3$	$9.2 \pm 2.5$	$6.5 \pm 1.5$
$i_R$ , deg	$-10.8 \pm 3.1$	$-13.1 \pm 3.5$	$-21 \pm 4$
$(\chi_\odot)_R$ , deg	$26 \pm 11$	$52 \pm 10$	$-8 \pm 4$
$\lambda_\theta$ , kpc	$2.7 \pm 0.5$	$2.6 \pm 0.7$	$4.8 \pm 1.4$
$f_\theta$ , km s <sup>-1</sup>	$8.9 \pm 2.5$	$9.6 \pm 2.7$	$7.5 \pm 1.5$
$i_\theta$ , deg	$-11.8 \pm 3.1$	$-11.6 \pm 3.8$	$-20 \pm 5$
$(\chi_\odot)_\theta$ , deg	$58 \pm 12$	$-51 \pm 12$	$12 \pm 6$

**Table 2.** Parameters of a spiral density wave found from samples of Cepheids from four age intervals in the past

Parameters	$t < 90$ Myr	$t : 90 - 120$ Myr	$t > 120$ Myr	Whole sample
$\lambda_R$ , kpc	$2.6 \pm 0.5$	$2.4 \pm 0.8$	$2.7 \pm 0.8$	$2.3 \pm 0.4$
$f_R$ , km s <sup>-1</sup>	$12.9 \pm 2.6$	$13.2 \pm 3.0$	$7.9 \pm 3.5$	$9.0 \pm 2.1$
$i_R$ , deg	$-11.6 \pm 3.4$	$-10.5 \pm 3.6$	$-11.8 \pm 3.3$	$-10.0 \pm 2.4$
$(\chi_\odot)_R$ , deg	$-74 \pm 15$	$-44 \pm 17$	$-73 \pm 18$	$-50 \pm 10$
$\lambda_\theta$ , kpc	$2.9 \pm 0.6$	$2.4 \pm 0.7$	$2.7 \pm 0.8$	$2.7 \pm 0.5$
$f_\theta$ , km s <sup>-1</sup>	$8.3 \pm 2.6$	$11.7 \pm 3.1$	$5.0 \pm 3.2$	$5.9 \pm 2.4$
$i_\theta$ , deg	$-12.7 \pm 3.5$	$-10.5 \pm 3.6$	$-11.8 \pm 3.3$	$-11.9 \pm 2.5$
$(\chi_\odot)_\theta$ , deg	$60 \pm 16$	$60 \pm 18$	$-33 \pm 14$	$-81 \pm 12$

dition of  $t \leq 90$  Myr. The average age of these relatively young Cepheids is  $\bar{t} = 66$  Myr.

The second sample contains 249 stars with ages from the interval 90–120 Myr. The average age of these Cepheids is  $\bar{t} = 105$  Myr.

The third sample contains 304 stars selected under the condition  $t > 120$  Myr. The average age of these Cepheids is  $\bar{t} = 165$  Myr.

Fig. 7 shows the  $X, Y$  distribution of three samples of Cepheids at the present time and in the past according to the age of each star. Parameters given on Fig. 7 of a four-arm spiral pattern were found by Bobylev & Bajkova (2014) from masers with measured trigonometric parallaxes. In the Figure, the following segments of spiral arms are numbered in Roman numerals: I – the Scutum arm, II – the Carina–Sagittarius arm, III – the Perseus arm, IV – the Outer arm.

The results of the spectral analysis of Cepheids are reflected in the Tables 1–2, as well as on Figures 8–11.

The Table 1 gives the parameters of the spiral density wave found from samples of Cepheids from three age intervals for the current moment of time. In the Table 2 similar values are given for four samples of Cepheids calculated for their past positions. In the Table 2 a column with the results obtained for the entire sample is added.

One of the most important parameters determining on the basis of spectral analysis is the wavelength  $\lambda$ . With the found value  $\lambda$ , the pitch angle  $i$  is calculated using the relation (13). As can be seen from the first and second columns of the Tables 1–2, for samples of Cepheids younger than 120 Myr, the values of  $\lambda$  lie in the range 2.4–3.0 kpc (this means that  $i$  is in the range  $[-13^\circ - 10^\circ]$  for a four-arm pattern model,  $m = 4$ ).

The values of  $\lambda_R$  and  $\lambda_\theta$ , found from a sample of

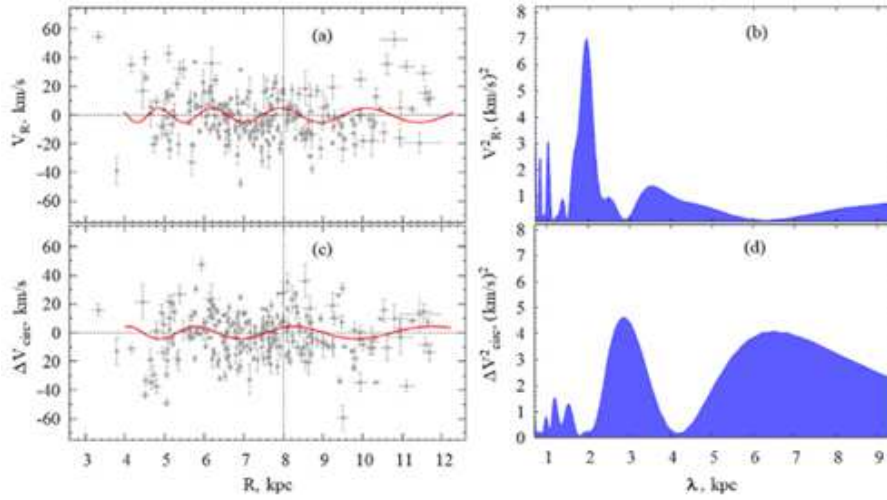
Cepheids older than 120 Myr for the current moment of time (Table 1), are very different from the similar values found from younger Cepheids. This problem is eliminated only in the case of an analysis of the velocities of the old Cepheids calculated at the time of their birth (Table 2 and Fig. 10–11).

Fig. 8 shows the radial  $V_R$  and residual tangential  $\Delta V_{circ}$  velocities at the present obtained for a sample of young ( $t \leq 90$  Myr) Cepheid and their spower spectra. For the same Cepheids, Fig. 9 gives the radial  $V_R$  and residual tangential  $\Delta V_{circ}$  velocities versus the distance  $R$  at the present time and in the past, where the periodic curves show the effect of a spiral density wave. The first column of the Table 1 gives the values of the spiral wave parameters found using the young ( $t \leq 90$  Myr) Cepheids. It should be noted that both for the sample of young Cepheids and for Cepheids of intermediate age, the values of the parameters of the spiral wave indicated in both tables are close. Therefore, illustrations for Cepheids of intermediate age are not given.

In Fig. 10, for the sample of old ( $t > 120$  Myr) Cepheids, radial  $V_R$  and residual tangential  $\Delta V_{circ}$  velocities are given at the present and their power spectra. The radial  $V_R$  and residual tangential  $\Delta V_{circ}$  velocities are given in Fig. 11 at the present time and in the past.

Another important parameter, to be determined on the basis of spectral analysis, is the amplitude of the perturbations  $f_R$  or  $f_\theta$ . If we take the peak values of the squares of velocities from the power spectra in Fig. 8 or Fig. 10, then the values  $f_R$  or  $f_\theta$  (indicated in the tables) can be found by the formula (16).

An analysis of modern data shows that in a wide region of the solar neighbourhood, the velocities  $f_R$  and  $f_\theta$  are



**Figure 8.** In the left-hand panel radial  $V_R$  (a) and residual tangential  $\Delta V_{circ}$  (c) velocities of young ( $t \leq 90$  Myr) Cepheids are shown. The velocities are given with error bars, the continuous periodic curves corresponding to the peaks of the power spectra (the spiral density wave) are given in red. The vertical dotted line marks the position of the Sun. In the right-hand panel the corresponding power spectra (b) and (d) are shown.

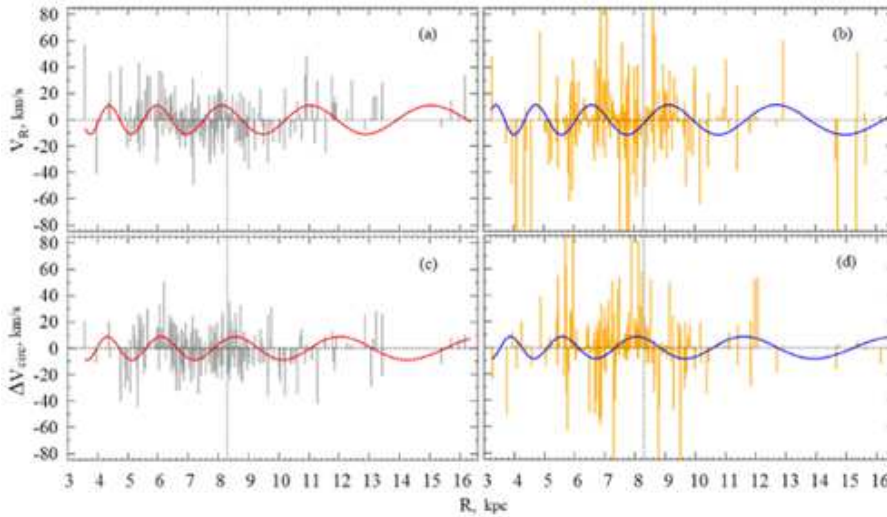


**Figure 9.** The radial  $V_R$  velocities of young ( $t \leq 90$  Myr) Cepheids at the present (a) and in the past (b), their residual tangential  $\Delta V_{circ}$  velocities at the present (c) and in the past (d). The continuous periodic curves corresponding to the peaks of the power spectra (the spiral density wave) are shown in red (in the present) and blue (in the past). The vertical dotted line marks the position of the Sun.

usually  $4\text{--}9 \text{ km s}^{-1}$ , and the wavelength  $\lambda$  is in the range  $2\text{--}3 \text{ kpc}$ .

Thus, from 130 maser sources with measured trigonometric parallaxes in the work of Rastorguev et al. (2017), there were found  $f_R = 6.9 \pm 1.4 \text{ km s}^{-1}$  and  $f_\theta = 2.8 \pm 1.0 \text{ km s}^{-1}$ , solar phase  $\chi_\odot = -125^\circ \pm 10^\circ$ . From 239 Galactic masers with measured trigonometric parallaxes in the work of Bobylev et al. (2020), there were found  $f_R = 7.0 \pm 0.9 \text{ km s}^{-1}$  and  $f_\theta = 3.8 \pm 1.1 \text{ km s}^{-1}$ .

From about 500 OB stars of the Gaia DR2 Catalog, Bobylev & Bajkova (2018) determined  $f_R = 7.1 \pm 0.3 \text{ km s}^{-1}$  and  $f_\theta = 6.5 \pm 0.4 \text{ km s}^{-1}$ ,  $\lambda_R = 2.3 \pm 0.2 \text{ kpc}$  and  $\lambda_\theta = 2.3 \pm 0.2 \text{ kpc}$ ,  $(\chi_\odot)_R = -135^\circ \pm 5^\circ$  and  $(\chi_\odot)_\theta = -123^\circ \pm 8^\circ$ . From sample of open clusters younger than 50

Myr, Bobylev et al. (2016) determined  $f_R = 7.7 \pm 1.4 \text{ km s}^{-1}$  and  $f_\theta = 5.6 \pm 1.6 \text{ km s}^{-1}$ ,  $\lambda_R = 2.1 \pm 0.5 \text{ kpc}$  and  $\lambda_\theta = 2.6 \pm 0.5 \text{ kpc}$ ,  $(\chi_\odot)_R = -85^\circ \pm 10^\circ$  and  $(\chi_\odot)_\theta = -62^\circ \pm 9^\circ$ .

From about 200 Cepheids from the Hipparcos Catalog, Bobylev & Bajkova (2012) found  $f_R = 6.8 \pm 0.7 \text{ km s}^{-1}$  and  $f_\theta = 3.3 \pm 0.5 \text{ km s}^{-1}$ ,  $\lambda = 2.0 \pm 0.1 \text{ kpc}$ ,  $\chi_\odot = -193^\circ \pm 5^\circ$ . We also note the new values of  $f_R = 4.6 \pm 0.7 \text{ km s}^{-1}$  and  $f_\theta = 1.1 \pm 0.4 \text{ km s}^{-1}$ , obtained in a recent work by Loktin & Popova (2019) from the analysis of modern data on Open Star Clusters.

Note that (Burton 1971) calculated the expected values for the perturbation velocities  $f_R \approx 8 \text{ km s}^{-1}$  and  $f_t \approx 6 \text{ km s}^{-1}$  for  $R = 8 \text{ kpc}$ .

The results of determining the  $f_R$ ,  $f_\theta$  and  $\lambda_R$ ,  $\lambda_\theta$

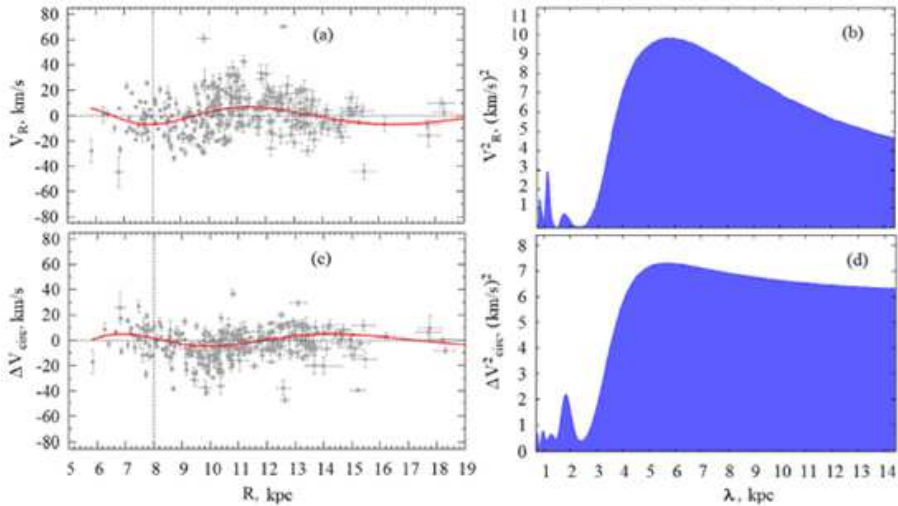


**Figure 10.** In the left-hand panel radial  $V_R$  (a) and residual tangential  $\Delta V_{circ}$  (c) velocities of old ( $t > 120$  Myr) Cepheids are shown. The velocities are given with error bars, the continuous periodic curves corresponding to the peaks of the power spectra (the spiral density wave) are given in red. The vertical dotted line marks the position of the Sun. In the right-hand panel the corresponding power spectra (b) and (d) are shown.

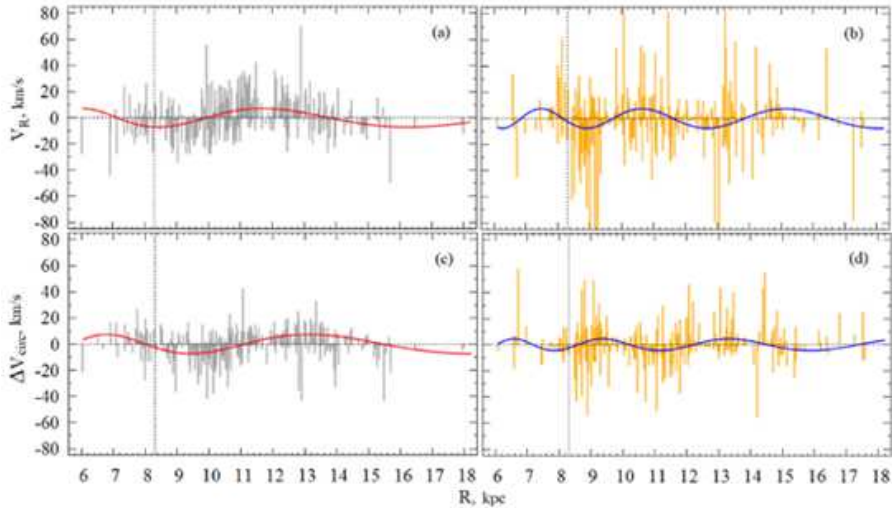


**Figure 11.** The radial  $V_R$  speeds of the old ( $t > 120$  Myr) Cepheids at the present (a) and in the past (b), their residual tangential  $\Delta V_{circ}$  speeds at the present (c) and in the past (d). The continuous periodic curves corresponding to the peaks of the power spectra (the spiral density wave) are shown in red (in the present) and blue (in the past). The vertical dotted line marks the position of the Sun.

by various authors are given in Fig. 12, where the results are marked with the following numbers: (1) – Rastorguev et al. (2017), (2) – Bobylev & Bajkova (2018), (3) – Bobylev & Bajkova (2012), (4) – Loktin & Popova (2019), (5) – Bobylev et al. (2020), (6) – Bobylev et al. (2016), (7) and black square – Burton (1971); results of this work from the last column of the table 2 are shown in blue, from first and second column of the table 1 are shown in gray.

Currently, there is no single generally accepted model of the spiral structure of the Galaxy. Theorists usually use the simplest two-arm model with a pitch angle of 5–7 degrees. Modern data on the distribution of clouds of neutral hydrogen, ionized hydrogen, and maser sources speak

rather of a four-arm model with a pitch angle of 10–14 degrees. Reviews on this issue can be found, for example, in the works Hou & Han (2014) or Vallée (2017c). In this paper, we adhere to the four-arm spiral pattern model with the parameters we found in previous works from the spatial and kinematical analysis of maser sources (Bobylev & Bajkova 2014).

In work of Dambis et al. (2015), an analysis of the spatial distribution of a large sample of classical Cepheids yielded estimates of the pitch angle of the four-arm spiral pattern  $i = -9.5^\circ \pm 0.1^\circ$  and the solar phase  $\chi_\odot = -121^\circ \pm 3^\circ$ .

The model of the global four-arm spiral pattern in the Galaxy is defended, for example, in the works of Vallée

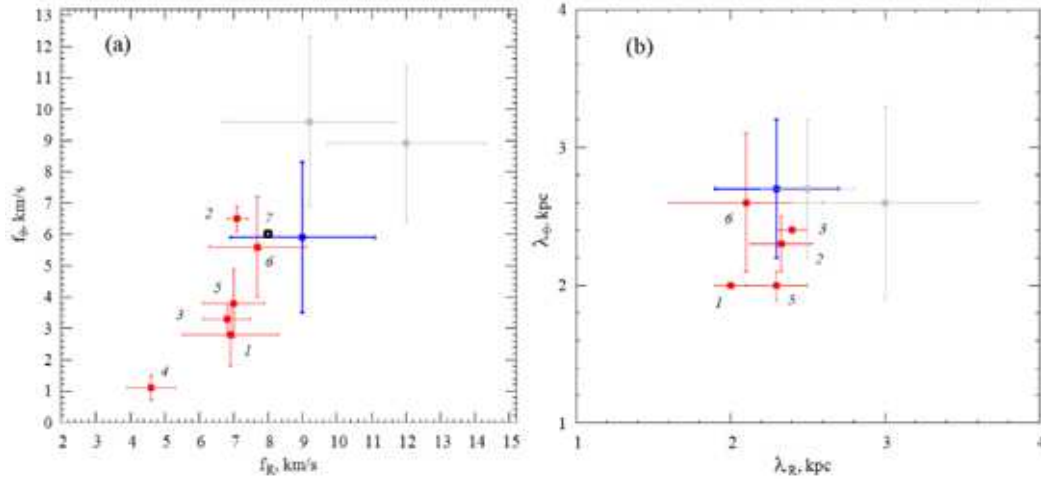


**Figure 12.** The results of determining the velocities  $f_R$  and  $f_\theta$  (a) and velocity  $\lambda_R$  and  $\lambda_\theta$  (b) by various authors – red and black, blue and gray – the result of this work, see also the text.

(2017b, 2018). Some authors prefer so far (before the appearance of more high-precision data) to consider individual segments of spiral arms with individual pitch angles (Nikiforov & Veselova 2018). In these models, the pitch angle lies in the range from  $-10^\circ$  to  $-15^\circ$ .

Light absorption strongly distorts the spatial distribution of objects and makes it difficult not only to determine their photometric distances, but also to calibrate the PLR even by high-precision trigonometric distances. To determine the absolute magnitude, it is necessary to know the color excesses, and for the Cepheids of the Milky Way this is a much more serious problem than for stars of constant brightness (Rastorguev et al. 2013; Lazovik & Rastorguev 2020) or for LMC Cepheids. Supposing a unified absorption law, we can solve these problems and reduce the effect of differential absorption by using two-color Wesenheit indices ( $W_{VI}$  as an example) instead of absolute magnitudes (Madore 1976). To use Wesenheit indexes of Cepheids instead of PLR, we should know the “period–normal color” relation, which reflects the shape and width of the instability strip and strongly depends on the metallicity of young populations. In addition, the use of Wesenheit indices or tricolor indices like  $Q_{UBV}$  to reduce the effects of differential absorption, is justified only for a small optical depth of dust in the broadband (heterochromic) photometry, which does not take place for Milky Way disk in optics.

The problem of calibrating PLRs and estimating photometric distances is additionally complicated by a noticeable difference in the absorption laws in the Milky Way galaxy (Fitzpatrick & Massa 2007, 2009), differing, first of all, by the value  $R_V = A_V/E_{B-V}$ , which varies from 2 to 6. That is why the photometric distances of the objects in the galactic disk, determined by optical data, can be strongly suffered from both random and hard-to-account for systematic errors.

It is for these reasons that in recent years, photometric data in NIR/MIR (2MASS, AllWISE, Spitzer and other projects) have been used to determine the photometric distances of objects, including Cepheids. For example, light absorption (expressed in magnitudes) in the  $K_s$  (2MASS) band

$A_{K_s} \approx 0.078(\pm 0.004) \cdot A_V$ , and in the WISE  $W1$ ,  $W2$  bands is  $A_{W1} \approx 0.039(\pm 0.004) \cdot A_V$  and  $A_{W2} \approx 0.026(\pm 0.004) \cdot A_V$  respectively Wang & Chen (2019). As is well known, average specific absorption  $a_V$  in the Galaxy plane is about  $1.5 \text{ mag kpc}^{-1}$  and, as a result, up to distances of 5 kpc in the  $W2$  band the absorption not exceed 0.20 mag (which is comparable with the internal scatter of PLR), and the effect of differences in the absorption laws is negligible at all. It should also be noted that the study of structures in the Galaxy, such as a spiral pattern, based on the spatial distribution of objects, is greatly affected by the selection effects due to interstellar extinction even in IR. However, these selection effects do not affect the kinematics at all, which justifies the kinematic analysis of the spiral structure performed in this paper.

As for microlensing effects, it should be borne in mind that for bulge stars this effect should be taken into account due to the huge number of observed stars (this is exactly what the results of the OGLE project discovered). The total sample size of Cepheids is negligible compared to the sample of bulge stars studied in OGLE, and even with the same lensing probability, the average expected number of lensings for the entire sample is much less than unity. Also, the lensing event itself, lasting some tens of days, in principle, could not distort either the estimate of the period (since the photometric monitoring of Cepheids lasts much longer than this time), or the results of precision astrometric measurements by Gaia, conducted for about 30 months.

Most recently, the latest version of the Gaia Early Data Release 3 (Brown et al. 2020; Lindegren et al. 2020) Catalog was published. It clarifies by about 30% the values of trigonometric parallaxes and proper motions for about 1.5 billion stars. The radial velocities are simply copied from the Gaia DR2 Catalog. We hope that the use of new data will not have a fundamental impact on the conclusions of this work.

Flat rotation curves of young objects reaching distances of about 15–20 kpc from the Galactic center, derived in numerous papers cited here, show an almost linear increase in the effective mass with the distance. A simple estimate of

the effective mass within a radius of 20 kpc for a rotation velocity of 220–230 km s<sup>-1</sup> leads to  $(2.3 \pm 0.3) \cdot 10^{11}$  solar masses. The main contribution even to this mass gives the dark matter, whose contribution only dominates with a further increase in distance. Its total contribution to the mass of the Galaxy and the local density of gravitating matter can be estimated only by modelling the gravitational potential, which takes into account the contribution of all structural components of the Galaxy to the rotation curve. In particular, this was done in the cited papers of Ablimit et al. (2020) and Bajkova & Bobylev (2016). In the latter paper the parameters of the density laws were derived from the kinematical study not only of disk objects, but also of very distant halo objects, and therefore they are considered as more reliable as compared to ones based only on objects within 15–20 kpc from the Galaxy center.

In this paper it was shown that the rotation curve of Cepheids is well approximated by the theoretical three-component model III from Bajkova & Bobylev (2016). Taking the estimates of the parameters of NFW model and the appropriate errors, we can easily derive an estimate of the contribution of DM to the total local density of gravitating matter:  $\rho_{DM} \approx 0.0114_{-0.0049}^{+0.0078} M_{\odot} \cdot \text{pc}^{-3}$ , which is 5 to 20% of the contribution of baryonic matter ( $0.101 M_{\odot} \cdot \text{pc}^{-3}$ ) according to the latest estimate made by the authors of the Besancon model of the Milky Way (Mor et al. 2018), based on the entire set of observational data. Our estimate of DM's contribution, in particular, is in excellent agreement with those of (Mor et al. 2018) ( $0.012 \pm 0.001 M_{\odot} \cdot \text{pc}^{-3}$ ); de Salas et al. (2019) ( $0.008 - 0.011 M_{\odot} \cdot \text{pc}^{-3}$ ) and Ablimit et al. (2020) ( $0.0105 \pm 0.0012 M_{\odot} \cdot \text{pc}^{-3}$ ). Note also that all the above estimates agree with an upper limit on the DM contribution to the local density in the Milky Way galaxy ( $0.027 M_{\odot} \cdot \text{pc}^{-3}$ ), made on the basis of a completely different approach – the analysis of galacto-vertical oscillations of Cepheids (Dambis 2004) and young open clusters (Dambis 2003).

## 5 CONCLUSIONS

The spatial and kinematic properties of a large sample of classical Cepheids with proper motions and line-of-sight velocities from the Gaia DR2 Catalog were studied. For this, we used data from the works of Mróz et al. (2019) and Skowron et al. (2019). The final sample contains about 800 Cepheids. For each of them there are estimates of distance and age as well.

The parameters of galactic rotation were found over the entire sample of Cepheids. So, the linear speed of rotation of the Galaxy at a solar distance amounted to  $V_0 = 240 \pm 3$  km s<sup>-1</sup>. Moreover, the distance from the Sun to the axis of rotation of the Galaxy was found to be equal to  $R_0 = 8.27 \pm 0.10$  kpc. We found that the distance scale correction factor  $p$  for both the entire sample and sub-samples of different ages has approximately the same value, equal to  $\sim 0.9$ . On this basis, it is concluded that the distances  $r$  of the analyzed Cepheids, calculated on the basis of the period-luminosity relation, must be extended by about 10%.

There was performed a spectral analysis of both radial  $V_R$ , and residual tangential velocities  $\Delta V_{circ}$  of Cepheid samples of different ages. For each sample, the parameters of the spiral density wave were obtained for two cases. In the

first case, spectral analysis was performed for the present moment of time. In the second case, the position and speed of the Cepheids were taken at the time of their birth. That is, a galactic orbit in the past was constructed for each star in accordance with an estimate of its age.

A spectral analysis of radial and tangential velocities showed that for samples of Cepheids younger than 120 Myr, both at the present time and in the past, we obtain close estimates of the parameters of the spiral density wave. So, the value of the wavelength  $\lambda_{R,\theta}$  lies in the range of [2.4–3.0] kpc, the pitch angle  $i_{R,\theta}$  in the range of  $[-13^\circ, -10^\circ]$  for the four-arm pattern model, the amplitude of the radial perturbations is  $f_R \sim 12$  km s<sup>-1</sup>, and the tangential perturbations are  $f_\theta \sim 9$  km s<sup>-1</sup>. These values are in agreement with the results of the analysis of other young objects of the Galaxy (for example, maser sources or OB stars).

But the sampling rates of older Cepheids (over 120 Myr) at the present time give the wavelength  $\lambda_{R,\theta} \sim 5$  kpc (hence  $i \sim 20^\circ$ ). This value contradicts the known results. This means that a lot of time has passed since the birth of these Cepheids in the spiral arms, they are significantly removed from their place of birth, and at present the sample does not have coherent properties. An analysis of positions and velocities of old Cepheids (more than 120 Myr), calculated by integrating their orbits backward in time, made it possible to determine significantly more reliable parameters of the spiral density wave: wavelength  $\lambda_{R,\theta} = 2.7$  kpc, amplitude of radial and tangential perturbations  $f_R = 7.9$  km s<sup>-1</sup> and  $f_\theta = 5$  km s<sup>-1</sup> respectively.

## ACKNOWLEDGMENTS

The authors would like to express their sincere gratitude to the anonymous referees for the interesting and useful remarks, the consideration of which made it possible to significantly improve the article. A. Rastorguev and M. Zabolotskikh are grateful to the Russian Foundation of Basic Research (Grant No. 19-02-00611) for partial financial support.

## DATA AVAILABILITY

The data underlying this article will be shared on reasonable request to the corresponding author.

## REFERENCES

- Abbott T.M.C., et al., 2019, ApJL 872, L30
- Ablimit I., Zhao G., Flynn C., and Bird S.A., 2020, ApJ 895L, 12
- Alard C., 2001, A&A 379, L44
- Anderson R.I., Saio H., Ekström S., et al., 2016, A&A 591, A8
- Babusiaux C., Gilmore G., 2005, MNRAS 358, 1309
- Bajkova A.T., Bobylev V.V., 2012, Astron. Lett. 38, 549
- Bajkova A.T., Bobylev V.V., 2016, Astron. Lett. 42, 567
- Benjamin R.A., Churchwell E., Babler B., et al., 2003, PASP, 115, 953
- Berdnikov L.N., Dambis A.K., and Vozyakova O.V., 2000, A&AS 143, 211

- Betoule M., Kessler R., Guy J., et al., 2014, *A&A*, 568, 22
- Bobylev V.V., Bajkova A.T., 2012, *Astron. Lett.* 38, 638
- Bobylev V.V., 2013a, *Astron. Lett.* 39, 753
- Bobylev V.V., 2013b, *Astron. Lett.* 39, 819
- Bobylev V.V., Bajkova A.T., 2014, *MNRAS* 437, 1549
- Bobylev V.V., Bajkova A.T., 2015, *MNRAS* 447, L50
- Bobylev V.V., Bajkova A.T., and Shirokova K.S., 2016, *Astron. Lett.* 42, 721
- Bobylev V.V., Bajkova A.T., 2018, *Astron. Lett.* 44, 675
- Bobylev V.V., Krisanova O.I., and Bajkova A.T., 2020, *Astron. Lett.* 46, 439
- Bono G., Marconi M., Cassisi S., et al., 2005, *ApJ* 621, 966
- Bhattacharjee P., Chaudhury S., and Kundu S., 2014, *ApJ* 785, 63
- Burton W.B., 1971, *A&A* 10, 76
- Camarillo T., Varun M., Tyler M., and Bharat R., 2018, *PASP* 130, 4101
- Caputo F., Marconi M., and Musella I., 2000, *A&A*, 354, 610
- Chemin L., Renaud F., and Soubiran C., 2019, *A&A*, 578, 14
- Churchwell E., Babler B., Meade M.R., et al., 2009, *PASP*, 121, 213
- Clemens D.P., 1985, *ApJ* 295, 422
- Dambis A.K., 2003, arXiv: astro-ph 030346
- Dambis A.K., 2004, Variable Stars in the Local Group, IAU Colloquium 193, Proc. of the conference held 6–11 July, 2003 at Christchurch, New Zealand. Eds D.W. Kurtz and K.R. Pollard. ASP Conference Proceedings 310. San Francisco: Astronomical Society of the Pacific, 158
- Dambis A.K., Berdnikov L.N., Efremov Yu.N., et al., 2015, *Astron. Lett.* 41, 489
- Do T., et al., 2019, *Science* 365, 664
- Efremov Yu.N., 2003, *Astron. Rep.* 47, 1000
- Feast M., Whitelock P., 1997, *MNRAS* 291, 683
- Fitzpatrick E.L., Massa D., 2007, *ApJ* 663, 320
- Fitzpatrick E.L., Massa D., 2009, *ApJ* 699, 1209
- Frink S., Fuchs B., and Wielen R., 1995, *Astron. Gesellschaft Abstract Ser.* 11, 196
- Gaia Collaboration, Prusti T., de Bruijne J.H.J., Brown A.G.A., et al., 2016, *A&A* 595, A1
- Gaia Collaboration, Brown A.G.A., Vallenari A., Prusti T., et al., 2018, *A&A* 616, A1
- Gaia Collaboration, Brown A.G.A., Vallenari A., Prusti T., et al., 2020, arXiv: 2012.01533
- Gaia Collaboration, Lindegren L., Hernandez J., Bombrun A., et al., 2018, *A&A* 616, 2
- Gaia Collaboration, Lindegren L., Klioner S.A., Hernández J., et al., 2020, arXiv: 2012.03380
- Gnaniński P., 2019, *AN* 340, 787
- Gravity Collaboration, Abuter R., Amorim A., Bauböck N., et al., 2019, *A&A* 625, L10
- Groenewegen M.A.T., 2018, *A&A* 619, A8
- de Grijs R., Bono G., 2017, *ApJS* 232, 22
- Griv E., Gedalin M., Pietrukowicz P., et al., 2020, *MNRAS*, 499, 1091
- Hammersley P.L., Garzon F., Mahoney T., and Calbet X., 1994, *MNRAS* 269, 753
- The Hipparcos and Tycho Catalogues, 1997, ESA SP–1200
- Hirota T., Nagayama T., Honma M., et al., 2020, *PASJ* 72, 50
- Hou L.G., Han J.L., 2014, *A&A* 569, 125
- Joy A.H., 1939, *ApJ* 89, 356
- Kawata D., Baba J., Ciuca I., et al., 2018, *MNRAS* 479, L108
- Lazovik Ya.A., Rastorguev A.S., 2020, *AJ* 160, 136
- Leavitt H.S., 1908, *Annals of Harvard College Observatory*, 60, 87
- Leavitt H.S., Pickering E.C., 1912, *Harvard College Observatory Circular*, 173, 1
- Lin C.C., Shu F.H., 1964, *ApJ* 140, 646
- Loktin A.V., Popova M.E., 2019, *Astrophys. Bulletin* 74, 270
- López-Corredoira M., Cabrera-Lavers A., and Gerhard O.E., 2005, *A&A* 439, 107
- Madore B.F., 1976, *RGOB* 182, 153
- Madore B.F., 1982, *ApJ* 253, 575
- Mainzer A., et al., 2011, *ApJ*, 731, 53
- Majaess D.J., Turner D.G., and Lane D.J., 2009, *MNRAS* 398, 263
- Majaess D., Dékány I., Hajdu G., et al., 2018, *Ap&SS*, 363, 127
- Mel’nik A.M., Dambis A.K., Rastorguev A.S., et al., 1999, *Astron. Lett.* 25, 518
- Mel’nik A.M., Rautiainen P., Berdnikov L.N., et al., 2015, *AN* 336, 70
- Metzger M.R., Caldwell J.A.R., and Schechter P.L., 1998, *AJ* 115, 635
- Mor R., Robin A.C., Figueras F., and Antoja T., 2018, *A&A* 620, 79
- Mróz P., et al., 2019, *ApJ* 870, L10
- Muraveva T., Delgado H.E., Clementini G. et al., 2018, *MNRAS* 481, 1195
- Nikiforov I.I., Veselova A.V., 2018, *Astron. Lett.* 44, 81
- Nishiyama S., et al., 2005, *ApJ* 621, L105
- Perlmutter S., et al., 1997, *ApJ* 483, 565
- Perlmutter S., et al., 1999, *ApJ* 517, 565
- Pojmański G., 2002, *Acta Astron.* 52, 397
- Pont F., Queloz D., Bratschi P., and Mayor, M., 1997, *A&A* 318, 416
- Rastorguev A.S., Dambis A.K., Zabolotskikh M.V., et al., 2013, “Advancing the Physics of Cosmic Distances”, Proc. IAU Symp. 289, 195
- Rastorguev A.S., Zabolotskikh M.V., Dambis A.K., Bajkova A.T., Bobylev V.V., 2017, *Astrophys. Bulletin* 72, 122
- Reid M.J., Dame N., Menten K.M., et al., 2019, *ApJ* 885, 131
- Riess A.G., et al., 1998, *AJ* 116, 1009
- Riess A., et al., 2004, *ApJ* 607, 665
- Riess A., et al., 2018a, *ApJ* 607, 665
- Riess, A.G., et al., 2018b, ArXiv: 1810.03526;
- Riess, A.G., et al., 2020, ArXiv: 2012.08534
- Ripepi V., Molinaro R., Musella I., et al., 2019, *A&A* 625, 14
- Röser S., Bastian, 1988, *A&AS* 74, 449
- Samus’ N.N., Kazarovets E.V., Durlevich O.V., et al., 2017, *Astron. Rep.* 61, 80
- Schmidt B.P., Suntzeff N.B., Phillips M.M., et al. 1998, *ApJ* 507, 46
- de Salas P.F., Malhan K., Freese K., et al., 2019, *Journal of Cosmology and Astroparticle Physics* 10, 37
- Sandage A., Tammann G.A., 2006, *ARA&A* 44, 93



- Schönrich R., Binney J., and Dehnen W., 2010, MNRAS 403, 1829
- Scolnic D.M., et al., 2018, ApJ, 859, 101
- Sedgwick T.M, Collins C.A., et al., 2021, MNRAS 500, 3728
- Skowron D.M., et al., 2019, Science 365, 478
- Stassun K.G., Torres G., 2018, ApJ Lett. 862, 61
- Turner D.G., 2012, JAVSO 40, 502
- Udalski A., Kubiak M., and Szymański M., 1997, Acta Astron. 47, 319
- Vallée J.P., 2017a, Ap&SS 362, 79
- Vallée J.P., 2017b, Astron. Review 13, 113
- Vallée J.P., 2017c, New Astron. Review 79, 49
- Vallée J.P., 2018, ApJ 863, 52
- Verde L., Treu T., and Riess A.G., 2019, Nature Astronomy 3, 891
- Wang S., Chen X., de Grijs R., et al., 2018, ApJ 852, 78
- Wang S., Chen X., 2019, ApJ 877, 116
- Wegg C., Gerhard O., and Portail M., 2015, MNRAS 450, 4050
- Wright E.L., et al., 2010, AJ 140, 1868
- Zabolotskikh M.V., Rastorguev A.S., and Dambis A.K., 2002, Astron. Lett. 28, 454
- Zinn J.C., Pinsonneault M.H., Huber D., and Stello D., 2019, ApJ 878, 136